Hardware Implementation and Real Time Performance Evaluation of Current Transformer Saturation Detection and Compensation Algorithms

Luis Alderete, Maria C. Tavares, Fabiano Magrin

***Abstract*—This paper presents a hardware implementation of two current transformer (CT) saturation detection methods and one distorted signal reconstruction method. Those methods have been implemented previously only in software. To evaluate the algorithms performance, a real time hardware in the loop system was implemented with several test scenarios forcing CT saturation.**

The paper highlights the influence of the quantization error generated by the analog-to-digital-converter in the reconstruction of distorted signal process and introduces a method to determine the best parameters to reconstruct the distorted current signal.

The methods used have shown precision and high speed in detecting and compensating distorted current signal in real time, even for the worst CT saturation cases.

***Keywords*—CT Saturation, Real Time Simulation, Detection, Distorted Signal Reconstruction, Hardware.**

I. Introduction

PROTECTION, control and substation automation using IEC 61850 standard has become a reality nowadays and the migration process to its full implementation is being carried out progressively. One of the most impacted sector by this standard is the Process Bus, where the instrument transformers outputs must have traditional cooper wiring replaced using local area network ethernet with appropriate data formatting to generate the sampled values [1]. The instrument transformers to be used for this purpose can be conventional type (CIT), that is, using ferromagnetic cores, and also the non-conventional instrument transformer (NCIT), called optical instrument transformer.

This modification is being done gradually by the electrical utilities mainly due to conventional instrument transformer life time, and due to conservative nature of protection engineers.

Conventional current transformers (CTs) which use ferromagnetic core are subject to magnetic saturation, that occurs based on the residual flux existing in the core before a short circuit event. Other factors such as DC component of short circuit current, burden and even wrong CT sizing can cause saturation. A saturated CT core distorts the secondary current waveform and due to it, protection relays are incorrectly sensitized, or even not sensitized at all, what that can generate a catastrophic situation for electrical system.

CT saturation affects directly some protection functions, as described below.

- Distance protection saturation effect (ANSI 21):

Distance protections are widely used in transmission and sub-transmission levels, as it has generally a low cost and a simple protection logic. According to [2], distance protection can be affected by CT saturation when calculating the fault impedance. The use of distorted signal can lead to under or overreach. According [3], directional element can also be affected due to CT saturation.

- Differential protection saturation effect (ANSI 87):

During external faults, CT saturation can generate incorrect currents that may be higher than the relay operating settings, that is, the relay can consider an external fault as an internal one, and operate improperly [4].

- Overcurrent protection saturation effect (ANSI 50/51):

Overcurrent protection uses the faulted phase current phasor magnitude to operate. When the signal provided by the CT is distorted due to saturation, the calculated magnitude will be lower than the real value, and this situation may cause a delay in the protection actuation [5].

Rebizant *et al.* [6], suggest some ways to avoid CT saturation such as increasing CT core cross section, use of air gap CT and algorithms to detect the beginning and end of saturation, then reconstruct the distorted current signal. The first solution, in addition to being an expensive solution, implies using large CT sizes that would not fit in the previously designated spaces. The second one involves using TPY and TPZ CT type that, according to [7], are uncommon for protection in most part of high-voltage transmission networks.

In order to explore the third suggested solution, which is a more economical approach, several saturation detection/compensation methods have been proposed in the technical literature. Some of them includes: (i) Application of neural networks (ANN): [8]-[9]-[10]; (ii) Use of Discrete Wavelet Transform (DWT): [11]; (iii) Comparison of the fundamental component and its scaled second and third derivative: [12]-[13].

This paper presents the main results obtained in the hardware implementation and real time performance evaluation of two algorithms that identifies the periods when CT saturation begins and ends, and the implementation of a distorted secondary CT signal reconstruction algorithm. The mentioned methods are not novel, and they were

This study was supported by the research agencies CAPES (code 001), CNPq and FAPESP (2017/20010-1).

Luis Alderete and Maria C. Tavares are with the School of Electrical and Computer Engineering, University of Campinas, Brazil (e-mail: luis.alderete@dsce.fee.unicamp.br; ctavares@unicamp.br),

Fabiano Magrin is with Federal University of Technology - Paraná (UTFPR), Curitiba Campus, Brazil (e-mail: magrin@utfpr.edu.br)

Paper submitted to the International Conference on Power Systems Transients (IPST2021) in Belo Horizonte, Brazil June 6-10, 2021.

implemented and evaluated in software before this work, but no study regarding hardware implementation have been provided previously.

Based on that, the contributions of this paper can be summarized as follow: (i) Hardware implementation of the cited methods; (ii) Establishment of a procedure to calculate the thresholds to identify the CT saturation region; (iii) Identify the influence of the quantization error introduced by analog-to-digital converter in the distorted signal reconstruction process; and (iv) Development of a methodology which determines the settings that correctly reconstruct the secondary distorted current signal.

The remainder of the paper is organized as follow. In section II, saturation detection and compensation methods are presented. Section III describes the hardware implementation using two RTDS racks for real-time testing. Section IV and V describes the results followed by a conclusion.

II. Theoretical Background

A. Saturation detection algorithms

In 2014, *Schettino et al.* [14] used a differentiating filter described by *Hamming* [15] in 1989 to analyze variations in the behavior of current signals at the transition points between saturated and unsaturated regions. According to the authors, one of the main characteristics of this algorithm is its efficiency for noise coming from electrical system.

The equation that describes the first difference function of the low-noise Lanczos filter applied to secondary CT current, referred here as *Lanczos*, is described below.

$$\begin{aligned} Lanczos[n] = -i_s[n] - 9.i_s[n-1] + 8.i_s[n-2] + \\ 8.i_s[n-3] - 9.i_s[n-4] + i_s[n-5] \end{aligned} \quad (1)$$

Where:

$i_s \rightarrow$ Secondary CT current

$n \rightarrow$ Value of the current for the n_{th} sample

Fig. 1 shows *Lanczos* algorithm applied to saturated CT secondary current. The saturation regions are associated to the peaks.

The second implemented algorithm is described below. In 1964, Savitzky and Golay [16] presented a smoothing and differentiation technique obtained experimentally and contaminated by noise through polynomial interpolation using the concept of least squares. The objective was to use this tool for data analysis in analytical chemistry area. *Schettino et al.* [16] applied those filters family in protection area in 2016. According to the authors, this filter has the characteristic of being immune to noise and frequency deviations.

The equation that describes Savitzky-Golay second-order differentiator filter, named here as *del2SG*, is described below.

$$\begin{aligned} del2SG[n] = \frac{1}{42}\{5.i_s[n] - 3.i_s[n-2] - 4.i_s[n-3] \\ -3.i_s[n-4] + 5.i_s[n-6]\} \end{aligned} \quad (2)$$

Where:

$i_s \rightarrow$ Secondary CT current

$n \rightarrow$ Value of the current for the n_{th} sample

Fig. 1 shows *del2SG* algorithm behavior applied to CT secondary current under saturation condition.

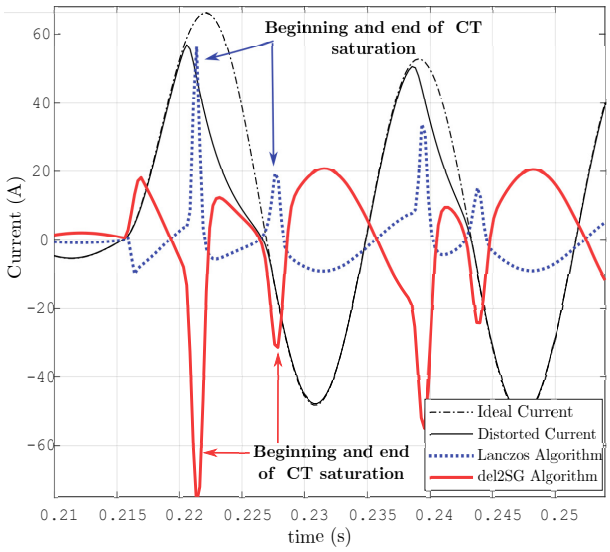

Fig. 1. Lanczos and Savitzky-Golay algorithms identifying CT saturation region

B. Compensation algorithm

The third algorithm implemented deals with waveform reconstruction. *Pan et al.* [17] proposed a compensation method for the distorted current portions through least squares method, which consist in utilizing healthy region samples to extract the primary current information. The method is explained as follow.

To estimate the compensated current, short-circuit current can be expressed as the combination of two components. The first one is short-circuit steady-state, or fault condition. The other component is the DC component generated at the instant of fault occurrence that will disappear according to system attenuation constant.

The equation that represents short-circuit current in a simplified power system is described by (3).

$$I_k = A.\cos\left(2.\pi.k\frac{f}{f_{samp}} + \varphi\right) + B.e^{\lambda k} \quad (3)$$

Where f_{samp} represents the sampling rate and f represents the power system frequency.

The unknown parameters (A, B, φ and λ) are calculated using least squares method to estimate secondary CT current in saturated regions. Equation (3) can be reformulated expanding cosine term through trigonometric identity and the exponential term can be replaced by first order Taylor series as in (4).

$$\begin{aligned} I_k = (A.\cos(\varphi)).\cos(\omega k) + (-A.\sin(\varphi)).\sin(\omega k) \\ +B + \lambda k \end{aligned} \quad (4)$$

Making $(A.\cos(\varphi)) = C_1$, $(-A.\sin(\varphi)) = C_2$ and using the angular frequency ω to represent $2.\pi.\frac{f}{f_{samp}}$, (5) is obtained.

$$I_k = C_1.\cos(\omega k) + C_2.\sin(\omega k) + B + \lambda k \quad (5)$$

Equation (5) can be formulated taking samples right before the saturated current portion of the sine wave signal, but not from pre-fault current. In (6), the current samples obtained from the unsaturated portion are numbered as k_i to $k_i + m_i$.

$$\begin{bmatrix} \cos\omega(k_i) & \sin\omega(k_i) & k_i & 1 \\ \cdots & \cdots & \cdots & \cdots \\ \cdots & \cdots & \cdots & \cdots \\ \cos\omega(k_i{+}m_i) & \sin\omega(k_i{+}m_i) & (k_i{+}m_i) & 1 \end{bmatrix} \cdot \begin{bmatrix} C_1 \\ C_2 \\ B \\ \lambda \end{bmatrix} = \begin{bmatrix} I(k_i) \\ \cdots \\ \cdots \\ I(k_i{+}m_i) \end{bmatrix} \tag{6}$$

A compact representation of (6) is given in (7), where **P** represents unknowns variables array. The reconstruction can be performed once **P** has been obtained.

$$\mathbf{MP} = \mathbf{I} \implies \mathbf{P} = (\mathbf{M^T M})^{-1}\mathbf{M^T I} \tag{7}$$

In each half-period that saturation occurs, new C_1, C_2, B and λ values are calculated (**P** vector) and replaced in (5). Then these current samples are used in the regions where the current is distorted due to saturation. C_1, C_2 contain information regarding AC waveform component, while B and λ values contain DC and exponential waveform information.

C. Establishing threshold for detection calculation

In this paper, the saturation threshold procedure developed by *Schettino et al.* [14], [16] was not implemented due to the high real time processing burden requirement. A new procedure was proposed, which consists of a simple, easy to implement in hardware and with a low computational burden characteristic.

The threshold establishment developed is based on real-time scanning of $Lanczos[n]$ or $del2SG[n]$ detector filters jointly with CT secondary current sample data, $I_2[n]$.

To understand the threshold definition process, in Fig. 2 it is observed that the saturation becomes smoother for the later semi-cycles after fault inception. Based on that, a threshold value was established for the onset saturation (named *TshUp*) and a ending saturation (named *TshDn*) for detection algorithm. These values were selected based on the smoothest saturation case, because the mildest case is also the most restrictive. It was possible then to detect the more severe saturation cases. To ensure that saturation was properly identified, a $I_2[n]$ threshold was implemented (named I_{2Tsh}), which is the secondary current value at which *TshUp* reaches the pre-established value.

Summarizing, the saturation begins if at sample $[n]$ the detector filter value is above *TshUp*, I_2 value is above I_{2Tsh} and at sample $[n-1]$ detector filter is below *TshUp*. A saturation end happens if at sample $[n]$ detector filter value is above *TshDn* and at sample $[n-1]$ detector filter value is below *TshDn*. The threshold values used for 64 sample/cycle were *TshUp*= 5 A, *TshDn*= 3 A and I_{2Tsh}= 28 A.

III. Test Environment

The presented algorithms performance was tested in a digital hardware in the loop (HIL) environment. Two RTDS racks were connected in parallel. The first one was used to implement a simplified electrical system (described in appendix), which consists of a 230 kV equivalent system connected to a circuit-breaker and a RL load. The CT was modeled with RTDS built-in Jiles-Atherton model, which can accurately represent CT ferromagnetic material behavior in steady state and transient conditions [18]. The second RTDS rack was used to create a component in the RTDS library that reads the current signal from rack 1 and processes the detection and reconstruction algorithms. The components were created using RTDS Component Builder software, and programmed in C language. Fig. 3 shows the hardware in the loop scheme mounted for performance tests using two RTDS racks.

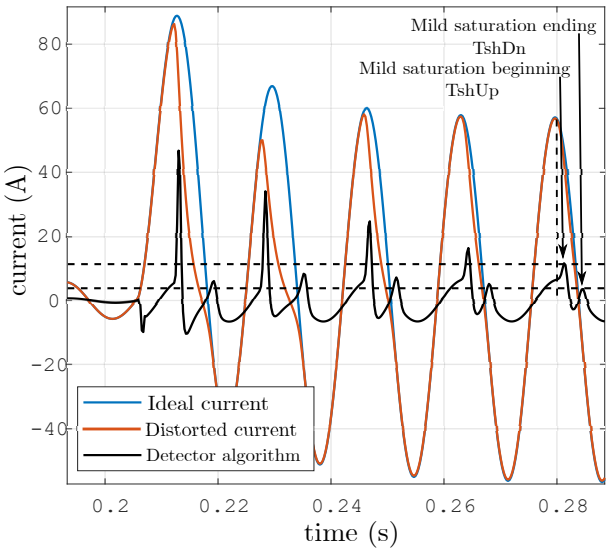

Fig. 2. *Threshold detection process*

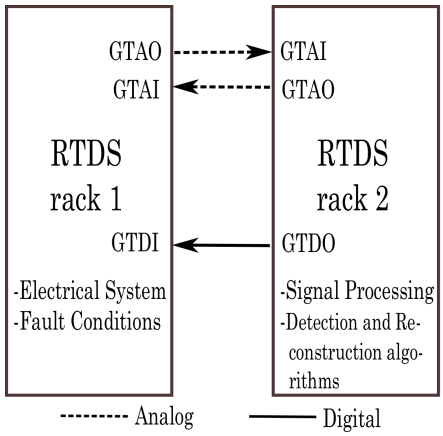

Fig. 3. Hardware in the loop scheme for algorithm performance tests (dashed line represents analog signal, continuous line represents digital signal)

IV. Results and Analysis

A. Tests

Tests were divided in two stages. First, the detection methods performances were evaluated, followed by the signal reconstruction method. All tests were performed using 64 samples per cycle, 1200 Hz cut-off frequency and 16-bit

analog-to-digital converter resolution, and considering severe, moderate and mild saturation conditions.

We proposed the use of a *Response Time* (RT) value to identify the beginning and end of saturation region. For signal reconstruction, RMS values of ideal, distorted and reconstructed current signals were compared.

1) Response Time (RT): The *Response Time* consists of measuring the time interval from the initial instant of the saturation to the instants obtained with each detection method. *RT* includes algorithms processing time, delays generated by low-pass filter and historical current samples. Fig. 4 shows the *Response Time* generated by the selected saturation detection algorithms.

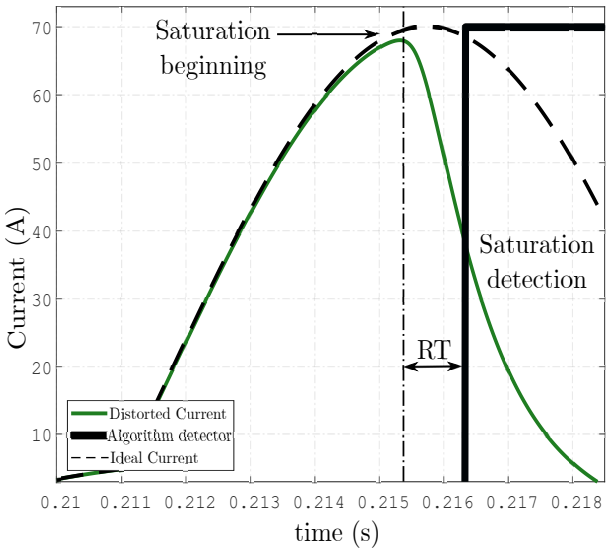

Fig. 4. *Response Time* identification

Tables I and II show the mean values results of 20 simulations considering severe, moderate and mild saturation simulations.

TABLE I
MEAN *Response Time* (RT) USING *Lanczos* DETECTION ALGORITHM

Lanczos Algorithm	
Saturation	Response Time (ms)
Severe	1.68
Moderate	1.73
Mild	1.78

TABLE II
MEAN *Response Time* (RT) USING *del2SG* DETECTION ALGORITHM

del2SG Algorithm	
Saturation	Response Time (ms)
Severe	2.12
Moderate	1.94
Mild	2.17

The obtained results indicate that both saturation detection algorithms are robust, with *RT* varying with the number of samples used. It is observed that *del2SG* algorithm had larger *Response Time* compared to *Lanczos* algorithm, what is expected as the number of historical samples are different (5 samples for *Lanczos* and 6 samples for *del2SG* case). It is also observed that saturation level slightly deteriorates the *Response Time*, but nothing relevant [19]-[20].

2) Reconstruction Process: Pan et al. [17] states that when a short circuit occurs, the secondary CT waveform current does not saturate for about 1/6 cycle in the first half cycle of the short-circuit and about 1/4 cycle between any two successive saturated waveform portions. This indicates that at least 10 healthy samples (64 samples/cycle) will be taken before CT saturates, representing the worst saturation case. Based on that, three variables were considered for distorted signal reconstruction process, as described below.

- Number of samples used for estimation (M) : Refers to the number of samples used to reconstruct distorted region, being necessary at least 5 samples to estimate the distorted signal.
- Bounce (d) : Is the spacing between the selected samples, can be 1, 2 or more (d=1 means consecutive samples are taken, no sample is skipped).
- Slack (g) : Refers to the distance, in samples, between the point where saturation is detected and the beginning of collected samples for reconstruction.

Fig. 5 shows the variables described above. For this case, the reconstruction parameter set used was M=5, d=2 and g=6.

It is important to highlight that when a given signal is sampled, A/D (analog-to-digital) converters introduce small errors called quantization errors, which leads to a signal information loss. It was observed during a bunch of test that even having the necessary number of pre-saturation samples to reconstruct the distorted signal, the A/D converter compromises the calculation of C_1, C_2, B and λ constants from (7), causing the reconstruct signal process to fail. Fig. 6 shows a case of improper signal reconstruction due to quantization error using 16 bits A/D converter.

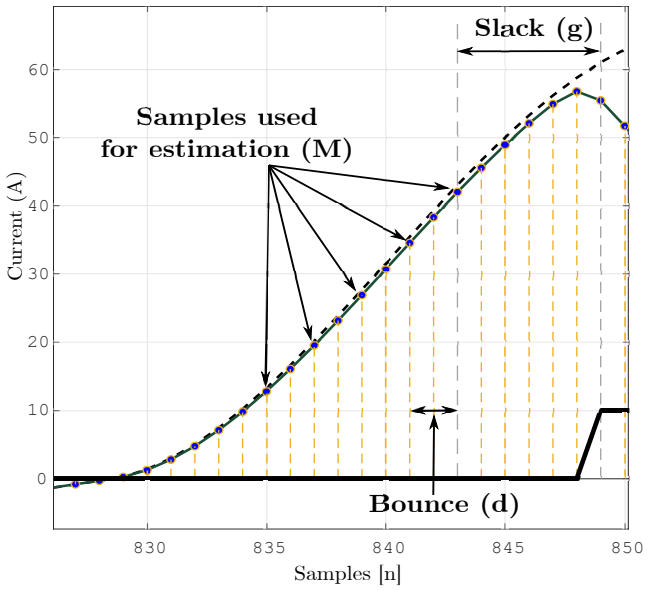

Fig. 5. Variables used for distorted signal reconstruction

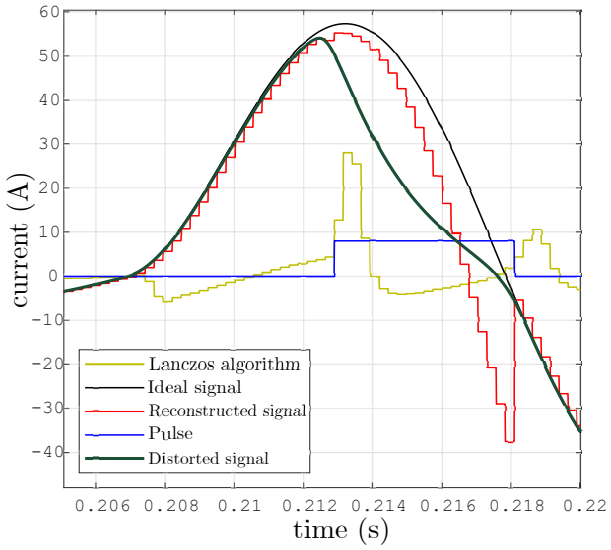

Fig. 6. Real-time incorrect reconstruction signal due to quantization error using 16 bits A/D converter

It was verified that increasing A/D converter resolution, or even without implementing A/D conversion process, the signal reconstruction was drastically improved. To demonstrate that, ideal and distorted CT signals were exported from RTDS simulator and used to reconstruct using Matlab without A/D converter process. Fig. 7 shows a perfect reconstruction signal using Matlab.

In order to overcome the problem and continue using a 16 bit A/D converter, as in commercial IEDs, a mathematical approach is presented. The process to find the appropriate M, g and d parameters that reconstruct properly a sinusoidal signal representing the secondary CT current was generated using Matlab. Parameters A and B from (3) were varied randomly from 10 to 150. Such signals were generated in a controlled manner, without saturation and with enough pre-fault samples so that M, g and d parameters could be analyzed without

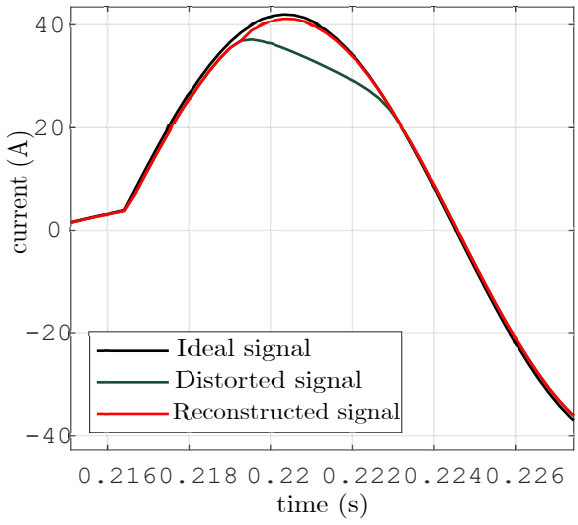

Fig. 7. Matlab distorted signal reconstruction without implementing analog-to-digital converter process

samples contamination.

The next step was to perform a statistical analysis varying M, g and d using the sinusoidal waveform previously described. The variables range were as follows: M between 5 and 7, d between 1 and 3 and g between 1 and 5. For each specific set of parameters, 500 simulations were performed. In each simulation, the mean value of maximum point-to-point error between ideal and reconstructed current was calculated. Also the standard deviation was analyzed.

Tables III to V show the simulations results. The highlighted values are the g and d parameters with the highest probability to reconstruct the distorted signal.

TABLE III
MEAN AND STANDARD DEVIATION VALUES FOR M = 5

$\overline{E}$		d			σ		d		
		1	2	3			1	2	3
g	1	19.44	45.96	21.80	g	1	19.04	3.73	1.30
	2	21.77	28.35	21.31		2	23.94	4.30	1.32
	3	21.43	15.85	21.36		3	22.68	3.06	1.32
	4	85.91	17.46	21.07		4	32.19	3.69	1.39
	5	88.94	18.22	26.61		5	30.83	4.15	1.79

TABLE IV
MEAN AND STANDARD DEVIATION VALUES FOR M = 6

$\overline{E}$		d			σ		d		
		1	2	3			1	2	3
g	1	13.72	14.71	23.84	g	1	10.56	1.50	0.77
	2	14.42	14.04	24.85		2	12.29	0.96	0.76
	3	50.42	14.15	27.70		3	13.76	0.34	0.81
	4	78.09	14.17	27.69		4	17.23	0.33	0.99
	5	84.43	14.50	30.39		5	17.28	1.55	0.86

TABLE V
MEAN AND STANDARD DEVIATION VALUES FOR M = 7

$\overline{E}$		d			σ		d		
		1	2	3			1	2	3
g	1	11.73	13.91	26.60	g	1	6.11	0.43	0.59
	2	32.82	13.94	27.57		2	7.93	0.29	0.58
	3	59.02	13.98	29.84		3	8.07	0.40	0.57
	4	19.66	14.16	29.97		4	7.96	0.89	0.47
	5	76.98	20.19	31.24		5	12.00	1.57	0.49

Fig. 8 shows a real time reconstruction of distorted signal for a severe saturation case (RTDS) applying the set of parameters obtained through the statistical analysis. A DC saturation can be observed during the former fault cycles, together with the saturation, producing the distorted secondary CT waveform due to inductive CT burden.

A good reconstruction is observed. The RMS magnitude values of ideal, reconstructed and distorted currents are also presented in Fig. 8 using a full cycle cosine filter. The reconstructed phasor magnitude matched the ideal (non-distorted) one.

Fig. 9 shows the reconstruction of distorted signal for a moderate saturation case (RTDS). This example is for a resistive-inductive CT burden. The reconstructed phasor

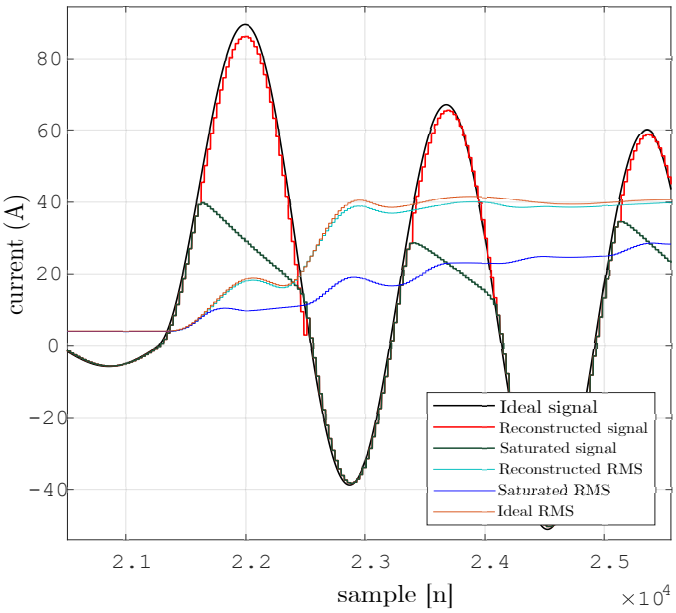

Fig. 8. Real time distorted signal reconstruction for a severe saturation case, with M=5, d=2 and g=3

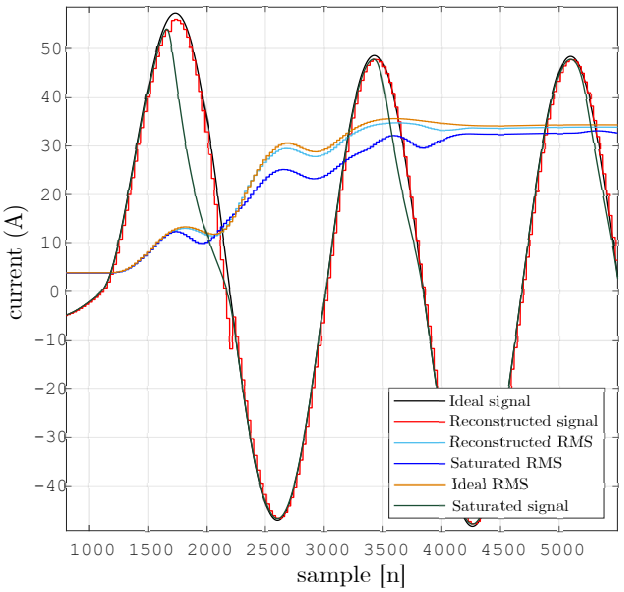

Fig. 9. Real time distorted signal reconstruction for a moderate saturation case, with M=5, d=2 and g=3

magnitude was again very close to ideal one, proving the good performance of the reconstruction algorithm.

The RTDS component created for processing detection and compensation algorithms consisted of the following stages:

- Low pass filtering,
- Down-sampling (reproducing precisely the A/D converter),
- Saturation detection algorithm,
- Distorted signal reconstruction algorithm,
- Phasor estimation (fundamental frequency) for the distorted and reconstructed signals.

The processing time of the cited stages using RTDS PB5 board varies between 3.3 to 3.5 μs and used 20 KB of memory.

The authors also evaluated the methods for different sampling rates, specifically 16, 32 and 128 samples per cycle. The saturation detection methods performed well using these sampling frequencies. The same did not occur for the reconstruction method for 16 and 32 samples per cycle due to insufficient fault current samples in the healthy region for the first half cycle. A good response was obtained for 128 samples/cycle, but with significant computational burden compared to the 64 samples/cycle.

V. Conclusions

This paper introduces a hardware implementation of a CT saturated current waveform reconstruction. The test was implemented in a real time hardware in the loop (HIL) environment with sampling rate and analog/digital (A/D) converter available in commercial relays, 64 samples/cycle and 16 bit, respectively. The computational burden was low, with a processing time below 5 μs.

Two different saturation detection methods were implemented, namely Lanczos and Savitzky-Golay (SG), that quickly and accurately detected the onset and end of different types/levels of CT saturation. Both methods had a good performance, but Lanczos was slightly faster. The detection response time is lower for high saturation level, and enlargers as saturation becomes mild. When higher sampling rate is applied the saturation detection time reduces. A good response was obtained even with 16 samples/cycle, but the time response slightly deteriorates.

The thresholds for identifying the saturation region with a 64 samples/cycle implementation was proposed.

The reconstruction method had an excellent response with a 64 sample/cycle rate for different saturation level. For higher sampling rate the computational burden increases. A minimum 16 bit A/D converter was identified to overcome the quantization error that prevented adequate signal reconstruction. This limitation prevented the use of lower sampling rate for the reconstruction stage.

The present implementation can be applied to protection functions that depends only on current phasor magnitude. It is also expected a good performance for applications which use the entire phasor (magnitude and angle), as the secondary CT current was properly reconstructed. Further material will be presented in near future with protection tests, as the methods can be implemented in commercial relays.

As a final remark, the authors understand that besides testing an algorithm through software simulation, it is essential to prove its effectiveness in a hardware in the loop environment. With HIL implementation it is possible to reproduce conditions much are similar to what is expected in real-life, and most important, identify inaccuracies that are more difficult to be provoked in software based conditions.

VI. Appendix

The power system modeled in RTDS is given in Fig. 10.

- Generator

Voltage Source (Phase-phase, RMS): 230 kV
Frequency: 60 Hz
Positive seq. series resistance: 20 Ω
Positive seq. parallel inductance: 80 mH

– Load
Resistance per phase: 300 Ω
Inductance per phase: 22 mH

– Current Transformer [21]
Transformation ratio: 180 (900/5)
Secondary winding resistance: 0.253 Ω
Secondary winding inductance: 0.8 mH
Load resistance: 20 Ω
Load inductance: 35 mH

CT Saturation Data:

Current (mA)	Voltage (V)
40	85
50	105
100	140
200	150
1000	160
10000	175

VII. References

[1] IEC Communication Network and Systems for Power Utility Automation, IEC Standard 61850-9-2, Specific communication service mapping (SCSM) – Sampled values over ISO/IEC 8802-3 Aug. 2004.

[2] Kinan Wannous and P. Toman, "The impact of current transformer saturation on the distance protection," 17th International Scientific Conference on Electric Power Engineering (EPE), 2016.

[3] Joe Mooney, "Distance element Performance Under Conditions of CT Saturation," 34th Annual Western Protective Relay Conference., Oct. 2007.

[4] H. Dashti, M. Sanaye-Pasand, M. Davarpanah, "Current transformer saturation detectors for busbar differential protection," 42nd International Universities Power Engineering Conference, 2007.

[5] I. M. El-amin and N. H. Al-abbas, "Saturation of Current Transformers and its Impact on Digital Overcurrent Relays," IEEE/PES Transmission Distribution Conference and Exposition: Latin America, 2006.

[6] Waldemar Rebizant, Janusz Szafran and Andrzej Wiszniewski, Digital Signal Processing in Power System Protection and Control, Springer, 2011,

[7] P. Stachel and P. Schegner, "Detection and correction of current transformer saturation effects in secondary current signals," IEEE Power Energy Society General Meeting, 2009

[8] W. Rebizant and D.Bejmert, "Current-transformer saturation detection with genetically optimized neural networks," in Proc. 2007 IEEE Trans Power Deliv., pp. 820-827.

[9] M. Saha and J.Izykowski and M Lukowicz and E Rosolowski, "Application of ANN method for instrument transformer correction in transmission line protection.," in Proc. 2001 IEE development in power system protection, pp. 303-306.

[10] D. Yu and J.Cummins and Z. Wang and H. Yoon and L. Kojovic, "Correction of current transformer distorted secondary current due to saturation using artificial neural networks," 2001 IEEE Trans Power Deliv., pp. 189-184.

[11] F. Li and R.Aggarwal, "Combined wavelet transform and regression technique for secondary current compensation of current transformer," 2002 IEEE Proc. Gener. Transm. Distrib., pp. 497-503.

[12] K. Chen and S. Glad, "Estimation of the primary current in a saturated transformer," 1991 30th conference on decision and control. Brighton, England, pp. 2363-2365.

[13] Y. Kang and S. Ok and S Kang, "A CT saturation detection algorithm," 2004 IEEE Transactions on Power Delivery, pp. 78-85.

[14] B. M. Schettino and C. A. Duque and P. M. Silveira and P. F. Ribeiro and A. S. Cerqueira, "A New Method of Current-Transformer Saturation Detection in the Presence of Noise," IEEE Trans. Power Delivery, vol. 29, pp. 1760-1767, 2014.

[15] Hamming, R. W., "Digital Filters", 3rd Ed., Ed. Prentice Hall International (UK) Ltd., 1989,

[16] B. M. Schettino and C. A. Duque and P. M. Silveira, "Current-Transformer Saturation Detection Using Savitzky-Golay Filter," IEEE Trans. Power Delivery, vol. 31, pp. 1400-1401, 2016.

[17] Jiuping Pan, Khoi Vu and Yi Hu, "An efficient compensation algorithm for current transformer saturation effects," IEEE Trans. Power Delivery, vol. 19, pp. 1623-1628, 2004.

[18] RTDS Technologies, "RSCAD Power System Component Manual," Winnipeg-Mb, CA, Nov. 2003

[19] L. Alderete, "Study of detection and compensation performance of a protection CT implemented in hardware (In Portuguese)," M.Sc. dissertation. University of Campinas, UNICAMP, 2020.

[20] L. Alderete and M. C. Tavares and F. Magrin, "Study of detection and compensation performance of a protection CT implemented in hardware (In Portuguese)," presented at the XXV National Electric Power Generation and Transmission Congress - SNPTEE, Belo Horizonte, Brazil, 2020.

[21] D. A. Tziouvaras and P. McLaren and G. Alexander and D. Dawson and J. Esztergalyos and C. Fromen and M. Glinkowski and I. Hasenwinkle and M. Kezunovic and L. Kojovic and B. Kotheimer and R. Kuffel and J. Nordstrom and S. Zocholl, "Mathematical models for current, voltage, and coupling capacitor voltage transformers. IEEE Transactions on Power Delivery, 2000.

[22] RTDS Technologies, "CBUILDER User's Manual - User Defined Component Models in C," Winnipeg-Mb, CA, April. 2012.

[23] RTDS Technologies, "RTDS NovaCor Hardware Manual," Winnipeg-Mb, CA, Nov. 2015

[24] K. Kumar and G. B. Kumbhar and S. Mahajan, "A New Efficient Algorithm to Detect Current Transformer Saturation," 2016 IEEE Power and Energy Society General Meeting (PESGM), pp. 1-5.

[25] S. R. Bhide, Digital Power System Protection, New Delhi: Asoke k. Ghosh, 2014.

[26] A. G. Phadke and J. S. Thorp, Computer Relaying for Power Systems - Second Edition, West Sussex: John Wiley ans Sons, 2009.

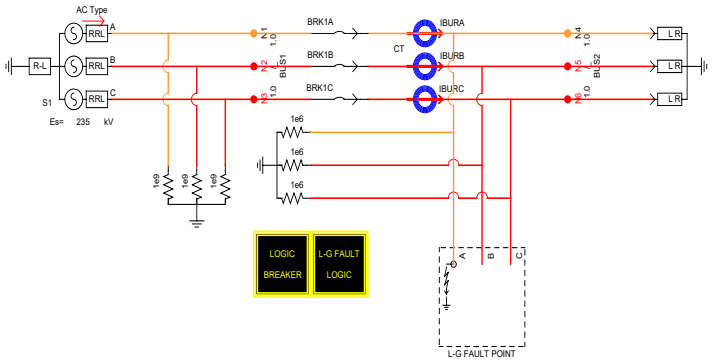

Fig. 10. Power system modeled in RTDS